

Symmetry Protected Topological Phases in Spin Ladders with Two-body Interactions

Zheng-Xin Liu,^{1,2} Zhen-Biao Yang,^{3,*} Yong-Jian Han,³ Wei Yi,^{3,†} and Xiao-Gang Wen^{2,4,‡}

¹*Institute for Advanced Study, Tsinghua University, Beijing, 100084, China*

²*Department of Physics, Massachusetts Institute of Technology, Cambridge, Massachusetts 02139, USA*

³*Key Laboratory of Quantum Information, University of Science and Technology of China, CAS, Hefei, Anhui, 230026, People's Republic of China*

⁴*Perimeter Institute for Theoretical Physics, Waterloo, Ontario, Canada N2L 2Y5*

Spin-1/2 two-legged ladders respecting inter-leg exchange symmetry σ and spin rotation symmetry D_2 have new symmetry protected topological (SPT) phases which are different from the Haldane phase. Three of the new SPT phases are t_x, t_y, t_z , which all have symmetry protected two-fold degenerate edge states on each end of an open chain. However, the edge states in different phases have different response to magnetic field. For example, the edge states in the t_z phase will be split by the magnetic field along the z -direction, but not by the fields in the x - and y -directions. We give the Hamiltonian that realizes each SPT phase and demonstrate a proof-of-principle quantum simulation scheme for Hamiltonians of the t_0 and t_z phases based on the coupled-QED-cavity ladder.

PACS numbers: 75.10.Pq, 64.70.Tg, 42.50.Pq

I. INTRODUCTION

Symmetry protected topological (SPT) phases are formed by gapped short-range-entangled quantum states that do not break any symmetry.¹ Contrary to the trivial case, quantum states in the non-trivial SPT phases cannot be transformed into direct product states via local unitary transformations which commute with the symmetry group. Meanwhile, two different states belong to the same SPT phase if and only if they can be transformed into each other by symmetric local unitary transformations.² A nontrivial SPT phase is different from the trivial SPT phase because of the existence of non-trivial edge states on open boundaries. This non-trivial property is protected by symmetry, because once the symmetry is removed, the SPT phases can be smoothly connected to the trivial phase without phase transitions.³ The well known Haldane phase⁴ is an example of SPT phase in 1-dimension (1D). Topological insulators⁵⁻¹⁰ are examples of SPT phases in higher dimensions.

The bosonic SPT phases are classified by projective representations (which describe the edge states at open boundaries or at the positions of impurities¹¹⁻¹³) of the symmetry group in 1D,¹⁴ and by group cohomology theory in higher dimensions.¹⁵ We also have a systematic understanding of free fermion SPT phases¹⁶ and some interacting fermion SPT phases.¹⁷⁻²⁰ Using those general results, fourteen new 1D SPT phases protected by D_2 spin rotation and time reversal symmetry are proposed in Ref. 21.

In this work, we will discuss two-legged spin-1/2 ladder models with two-body anisotropic Heisenberg interactions respecting $D_2 \times \sigma$ symmetry. Here σ is the inter-chain exchanging symmetry and $D_2 = \{E, R_x, R_y, R_z\}$, where E is the identity, $R_x (R_y, R_z)$ is a 180° rotation of the spin along $x (y, z)$ direction. The symmetry $D_2 \times \sigma$ protects seven non-trivial SPT phases. Four of them, t_0, t_x, t_y, t_z , can be realized in spin-1/2 ladder models. The t_0 phase is the Haldane phase, and the t_x, t_y, t_z phases

are new because of their different edge states. We provide a simple two-body Hamiltonian for each SPT phase, and study the phase transitions between these phases. We also discuss possible physical realizations of the SPT Hamiltonians and demonstrate a proof-of-principle implementation scheme based on coupled quantum electrodynamics (QED) cavity ladder.

The paper is organized as follows: in Sec. II, we introduce the projective representations of the underlying symmetry group of the two-legged spin-1/2 ladder and discuss the possible SPT phases. We then numerically study the phase diagram and the phase transitions of the spin-ladder Hamiltonians in Sec. III. In Sec. IV, we discuss the physical realizations of the SPT Hamiltonians and demonstrate a proof-of-principle quantum simulation scheme based on QED cavity ladder. Finally, we summarize in Sec. V.

II. PROJECTIVE REPRESENTATIONS OF THE SYMMETRY GROUP AND SPT PHASES

The symmetry group $D_2 \times \sigma$ for our two-legged spin-1/2 ladder is Abelian. All its eight representations are 1-dimensional. The following two-spin states on a rung form four different 1D representations of the symmetry group: $|0, 0\rangle = \frac{1}{\sqrt{2}}(|\uparrow_1\downarrow_2\rangle - |\downarrow_1\uparrow_2\rangle)$, $|1, x\rangle = \frac{1}{\sqrt{2}}(|\downarrow_1\downarrow_2\rangle - |\uparrow_1\uparrow_2\rangle)$, $|1, y\rangle = \frac{i}{\sqrt{2}}(|\downarrow_1\downarrow_2\rangle + |\uparrow_1\uparrow_2\rangle)$, and $|1, z\rangle = \frac{1}{\sqrt{2}}(|\uparrow_1\downarrow_2\rangle + |\downarrow_1\uparrow_2\rangle)$. The subscripts 1, 2 label the different spins on the same rung. The group $D_2 \times \sigma$ has eight projective representations (see Tab. I), which describe eight different SPT phases²² of spin ladder models.¹⁴ One of the projective representations is one-dimensional and trivial. The other seven non-trivial ones are two-dimensional, which describe the seven kinds of two-fold degenerate edge states of the seven non-trivial SPT phases.

The degeneracy at the edge in each non-trivial SPT

TABLE I: Projective representations and the corresponding SPT phases for $D_2 \times \sigma$ group. The active operators can split the degeneracy of the ground states. The operator $O_{\pm} = O_1 \pm O_2$, where 1,2 are the labels of the two spins at a rung, and SS_- means $\mathbf{S}_{1,i} \cdot \mathbf{S}_{1,i+1} - \mathbf{S}_{2,i} \cdot \mathbf{S}_{2,i+1}$.

	R_z	R_x	σ	active operators	SPT phases
E_0	1	1	1		rung-singlet ^a , $t_x \times t_x, \dots$
E_1	1	$i\sigma_z$	σ_y	(S_-^z, S_+^z, SS_-)	$t_x \times t_y$
E_2	σ_z	1	$i\sigma_y$	(S_-^x, S_+^x, SS_-)	$t_y \times t_z$
E_3	$i\sigma_z$	σ_x	1	(S_+^x, S_+^y, S_+^z)	$t_0, t_x \times t_y \times t_z$
E_4	σ_z	$i\sigma_z$	$i\sigma_x$	(S_+^y, S_-^y, SS_-)	$t_x \times t_z$
E_5	$i\sigma_z$	σ_x	$i\sigma_x$	(S_+^x, S_+^y, S_+^z)	t_x
E_6	$i\sigma_z$	$i\sigma_x$	σ_z	(S_-^x, S_-^y, S_+^z)	t_z
E_7	$i\sigma_z$	$i\sigma_x$	$i\sigma_y$	(S_-^x, S_+^y, S_-^z)	t_y

^aIf the system has translational symmetry, there are four different rung-singlet phases: rung- $|0, 0\rangle$ phase, rung- $|1, x\rangle$ phase, rung- $|1, y\rangle$ phase and rung- $|1, z\rangle$. If the system does not have translational symmetry, then there is no difference between the four rung-singlet phases and there will be only one rung-singlet phase.

phase is protected by the symmetry. To lift such a degeneracy, we need to add perturbations to break the $D_2 \times \sigma$ symmetry. The operators that split the edge degeneracy are called active operators.²¹ The active operators are different in different SPT phases, which provide experimental methods to probe different SPT phases.

We will mainly study five of the eight SPT phases which can be realized in two-legged spin-1/2 ladders: one trivial SPT phase (corresponding to E_0) and four non-trivial ones t_0, t_x, t_y, t_z (corresponding to E_3, E_5, E_6, E_7 respectively). The t_0 phase is equivalent to the spin-1 Haldane phase, where the edge states behave like a spin-1/2 spin and will be polarized by a magnetic field in arbitrary direction. However, in the t_z phase, the edge states will only respond to the z component of a homogeneous magnetic field ('homogeneous' means that the field takes the same value at the two sites of a rung). That is to say, the ground state degeneracy will be lifted by B_z but not by B_x or B_y (see Appendix A). The t_x and t_y phases are defined similarly. From the response of the edge states to external magnetic field, we can distinguish the four phases t_0, t_x, t_y, t_z .²³

The other three SPT phases can be realized by stacking two of the above ones: the SPT phases corresponding to E_1, E_2, E_4 can be realized by stacking t_x and t_y, t_y and t_z, t_x and t_z , respectively. The t_0 phase can also be realized by stacking three phases t_x, t_y, t_z .

The nontrivial SPT phases t_0, t_x, t_y, t_z can be realized in two-legged spin-1/2 ladders. The Hamiltonian that realize these phases is simply given as $H = H_L + H_T$, where H_L is the interaction along the leg (or longitudinal direction) and H_T is the interaction along the rung (or transverse direction). We assume H_L takes the following

form,

$$H_L = J \sum_i [(\delta S_{1,i}^x S_{1,i+1}^x + S_{1,i}^y S_{1,i+1}^y + S_{1,i}^z S_{1,i+1}^z) + (\delta S_{2,i}^x S_{2,i+1}^x + S_{2,i}^y S_{2,i+1}^y + S_{2,i}^z S_{2,i+1}^z)],$$

where $J > 0$, $\delta \sim 1$, and $S_{j,i}^m$ ($m = x, y, z$) is the spin operator at the j th leg and i th rung.

By tuning the interaction H_T , we can obtain four SPT phases t_0, t_x, t_y, t_z . For example, the following model

$$H_0 = H_L + \lambda \sum_i \mathbf{S}_{1,i} \cdot \mathbf{S}_{2,i}. \quad (1)$$

can realize the t_0 phase. When $\lambda > 0$, the rung-singlet state ($|0, 0\rangle$) is lower in energy and the system falls into the rung- $|0, 0\rangle$ phase, which is a trivial SPT phase. When $\lambda < 0$, the rung-triplet ($|1, x\rangle, |1, y\rangle, |1, z\rangle$) are lower in energy, and effectively we obtain a spin-1 anisotropic Heisenberg model, which belongs to the Haldane phase t_0 .

By partially flipping the sign of interactions along the rung, we obtain the Hamiltonian for the t_z phase:

$$H_z = H_L + \lambda \sum_i (-S_{1,i}^x S_{2,i}^x - S_{1,i}^y S_{2,i}^y + S_{1,i}^z S_{2,i}^z). \quad (2)$$

When $\lambda > 0$, it falls into a trivial SPT phase which corresponds to the rung $|1, z\rangle$ product state. When $\lambda < 0$, the low energy degrees of freedom in each rung are given by three states $|1, x\rangle, |1, y\rangle, |0, 0\rangle$, and the resultant model belongs to the t_z phase. Note that the Hamiltonians (1) and (2) (with the respective ground states t_0 and t_z) can be transformed into each other by the unitary transformation: $U_1(\pi) = \exp(i\pi \sum_i S_{1,i}^z)$. However, this does not mean that t_0 and t_z belong to the same phase since $U_1(\pi)$ does not commute with the symmetry group $D_2 \times \sigma$. Applying similar arguments, we may have $H_x = H_L + \lambda \sum_i (S_{1,i}^x S_{2,i}^x - S_{1,i}^y S_{2,i}^y - S_{1,i}^z S_{2,i}^z)$ for the t_x phase, and $H_y = H_L + \lambda \sum_i (-S_{1,i}^x S_{2,i}^x + S_{1,i}^y S_{2,i}^y - S_{1,i}^z S_{2,i}^z)$ for the t_y phase. Tab. I shows that different SPT phases have different active operators. For example, in the t_0 phase, the edge degeneracy can be lifted by either S_+^x or S_+^y or S_+^z . This means that the edge states can be polarized by a homogeneous magnetic field along any direction. In the t_z phase, S_+^x and S_+^y are not active operators, indicating that a weak homogeneous magnetic field in the x - y plane will not split the edge degeneracy. These properties can be verified by a finite-size exact diagonalization study of the Hamiltonian (1) and (2).²¹

III. PHASE TRANSITIONS AND THE PHASE DIAGRAM

To study the phase transitions, we consider the following model which contains both t_0 and t_z phases,

$$H = H_L + \sum_i [\lambda_{xy} (S_{1,i}^x S_{2,i}^x + S_{1,i}^y S_{2,i}^y) + \lambda_z S_{1,i}^z S_{2,i}^z]. \quad (3)$$

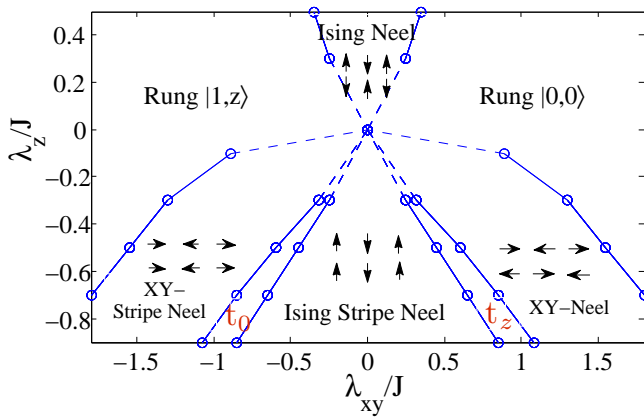


FIG. 1: (Color online) The phase diagram of the λ_z - λ_{xy} plane with $\delta = 0.9$. The point $(\lambda_{xy}, \lambda_z) = (0, 0)$ is a multi-critical point. Near this point, the phase boundaries are hard to determine. The dashed line means that the phase boundaries are not accurate. The two ‘XY’ phases are gapped and magnetically ordered in y -direction because $\delta \neq 1$ introduces anisotropy in the x - y plane. The t_0/t_z SPT phase locates between an Ising-type ordered phase and an XY-type ordered phase.

Since the λ_{xy} - λ_z plane phase diagrams of above model are quite different for $\delta \neq 1$ and $\delta = 1$, we will discuss them separately.

A. the case $\delta \neq 1$

1. The phase daigram

We only consider the case that anisotropy is weak, so we set $\delta = 0.9$ for simplicity. The phase diagram Fig. 1 (with $\delta = 0.9$) is obtained via infinite time-evolving block decimation (iTEBD) algorithm.²⁴ The phase diagram is symmetric along the line $\lambda_{xy} = 0$, because the model with $-\lambda_{xy}$ can be obtained from the one with λ_{xy} by the unitary transformation $U_1(\pi)$. The origin $(\lambda_{xy}, \lambda_z) = (0, 0)$ is a multi-critical point linking all the phases. On the upper half plane $\lambda_z > 0$, there are only three phases. The lower half plane is more interesting. The limit $\lambda_z \rightarrow -\infty$ corresponds to the Ising Stripe-Neel phase, while $\lambda_{xy} \rightarrow \pm\infty$ corresponds to the rung- $|0, 0\rangle$ /rung- $|1, z\rangle$ phase.

In the intermediate region, we have two XY-like phases and two SPT phases: XY-stripe Neel phase and XY-Neel phase. For $\delta \neq 1$, the exchange interactions along the legs are anisotropic in the x - y plane, consequently the two XY-like phases have a finite excitation gap and are ordered in y -direction if $\delta < 1$ (or ordered in x -direction if $\delta > 1$). The t_0/t_z phase is located between the XY-stripe Neel/XY-Neel phase and the Ising stripe Neel phase. The phase diagram at $\lambda_z = -0.5J$ is also shown in Fig. 2, where we illustrate the symmetry breaking orders and the entanglement spectrum ($\Delta\rho = \rho_1 - \rho_2$ is the difference be-

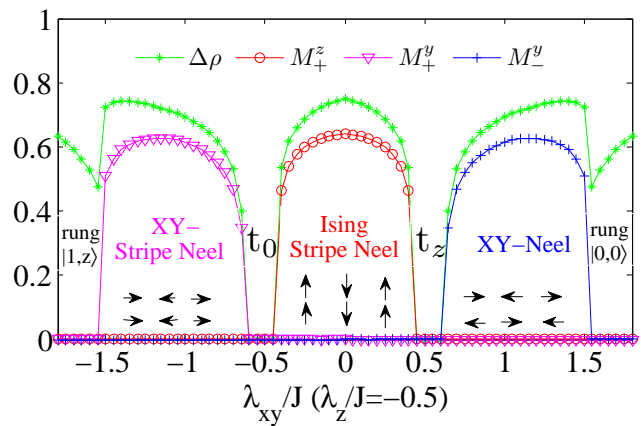


FIG. 2: (Color online) Phase transitions with $\delta = 0.9$, $\lambda_z = -0.5J$. The order parameters are defined as $M_{\pm}^m = |\langle S_1^m \pm S_2^m \rangle|$. The green line with asterisks shows the information of entanglement spectrum $\Delta\rho = \rho_1 - \rho_2$, where ρ_1 and ρ_2 are the two maximum Schmidt eigenvalues of the ladder, $\Delta\rho = 0$ means that the entanglement spectrum is doubly degenerate. The SPT phases are characterized by doubly degeneracy in the entanglement spectrum and vanishing of all magnetic orders.

tween the two biggest Schmidt eigenvalues) in each phase. For $\delta = 1$, the two XY phases vanish, and the SPT phase t_0/t_z touches the trivial phase rung- $|1, z\rangle$ /rung- $|0, 0\rangle$ directly (we will study this case in detail later).

2. Semiclassical explanation of the phase diagram

Notice that both of the SPT phases are sandwiched by two ordered phases. This suggests that they originate from quantum fluctuations caused by the competition between the different classical orders. To understand this point better, it will be interesting to compare the phase diagram Fig. 1 with that from the semiclassical approach in which the ground state is approximated by a direct product state. A semiclassical phase diagram (Fig. 3 with $\delta = 0.9$, $\lambda_z = -0.5J$) is obtained by minimizing the energy of the following trial wave function,

$$|\psi\rangle_{sc} = \prod_i (a_1\phi_{1,2i} + a_2\phi_{2,2i} + a_3\phi_{3,2i} + a_4\phi_{4,2i}) \\ \otimes (a_2\phi_{1,2i+1} + a_1\phi_{2,2i+1} - a_3\phi_{3,2i+1} + a_4\phi_{4,2i+1}),$$

where $\phi_1 = -\frac{1}{\sqrt{2}}(|1, x\rangle + i|1, y\rangle)$, $\phi_2 = \frac{1}{\sqrt{2}}(|1, x\rangle - i|1, y\rangle)$, $\phi_3 = |1, z\rangle$, $\phi_4 = |0, 0\rangle$ are four bases of each rung, and a_1, a_2, a_3, a_4 are four trial parameters.

Comparing the semiclassical phase diagram with Fig. 2, we find that the two phase diagrams are similar except for the absence of two SPT phases in Fig. 3. Importantly, the locations of the quantum SPT phases are close to the phase boundaries between the Ising ordered phase ($M_{\pm}^z \neq 0$) and the xy -planar ordered phases ($M_{\pm}^y \neq 0$) of the semiclassical phase diagram. Similar

situations occur in spin-1 XXZ chain, where a Haldane phase exists between two ordered phases.^{1,25} This suggests that we can roughly obtain a quantum phase diagram with a semiclassical approach by ‘inserting’ a SPT phase at the phase boundary of two different classically ordered phases.

Furthermore, the semiclassical picture even indicates some important information of the quantum SPT phases. For instance, it tells us why the t_0 phase is different from the t_z phase. The classical phase boundary between the two ordered phases is located at $|\lambda_{xy}^c| = |\lambda_z|$. At the point $\lambda_{xy}^c = \lambda_z < 0$, the states have the same lowest energy if the spins are antiferromagnetically ordered along the leg and are parallel along the rung polarizing in y - z plane (namely, the classical ground states are highly degenerate). Quantum fluctuations (which is enhanced by the degeneracy) will drive the system into the higher energy states (e.g. some spins are pointing off the y - z plane) with a certain weight. As a consequence, the ground state is short-range correlated with a finite excitation gap. Furthermore, edge states exist at each boundary. The edge states can be considered as an effective spin whose magnetic momentum is half of the total momentum of the two spins at a rung. Since the two spins in the same rung are parallel, the edge states carry free magnetic moment and respond to magnetic field along arbitrary directions. On the other hand, at the point $\lambda_{xy}^c = -\lambda_z > 0$, the lowest energy classical states are those that the two spins are parallel along the z direction and anti-parallel in the x - y plane (see Fig. 4b). Quantum fluctuations around the sphere drive this state to the t_z phase. In the t_z phase, the effective edge spins have no net magnetic moment in the x - y plane, so they will not respond to the magnetic field in the x - y plane. Similar things happen in the t_x and t_y phases. Above arguments are applicable to other systems with different SPT symmetry groups, and provide a guidance to seek SPT phases and analyze their physical properties.

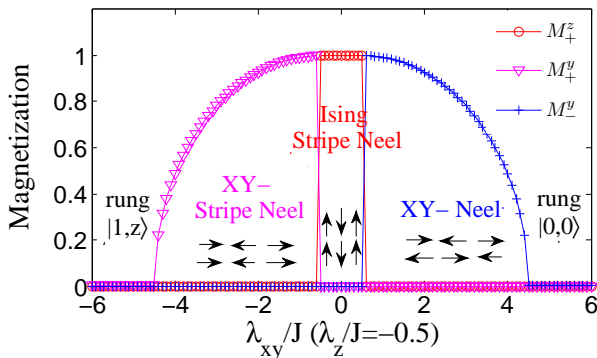


FIG. 3: (Color online) The order parameters M_+^z and M_\pm^y in the semiclassical approach. Compared to Fig. 2, the two SPT phases are missing.

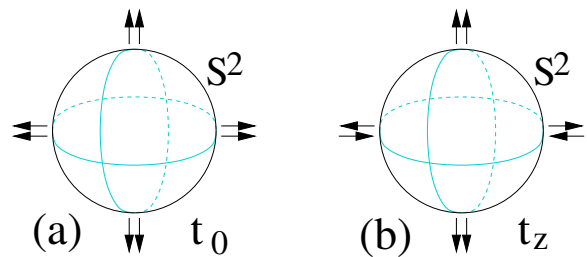


FIG. 4: (Color online) (a) At $\lambda_{xy}^c = \lambda_z < 0$, the classical states on the sphere are close in energy. Each direction on the sphere defines a classical state in which two spins at the same rung are parallel and pointing in that direction. (b) At $\lambda_{xy}^c = -\lambda_z > 0$, the classical states on the sphere are also nearly degenerate. But now the two spins at the same rung are antiparallel in the x - y plane and parallel off the plane.

B. the case $\delta=1$

1. Finite size effect in numerical method

When establishing the phase diagram Fig. 1 and Fig. 2, we have approximated the ground state by a matrix product state (MPS), which is obtained through iTEBD method.²⁴ The matrices in the MPS have a finite dimension D , which introduces a cutoff to the number of Schmidt eigenvalues in the entanglement Hilbert space. While the energy of the actual ground state can be estimated using a finite- D MPS with high accuracy, the order parameters are usually overestimated due to the finite dimension of the matrix. Furthermore, in some cases the order parameters (which are finite if D is finite) even vanish in the infinite D limit. So a scaling of the order parameters with respect to the dimension D is necessary in order to obtain the correct phase diagram. In the following we will illustrate, via finite size scaling, that the two XY phases disappear if $\delta = 1$.

The phase diagram in Fig. 5(a) with $\delta = 1$, $\lambda_z = -0.5J$ is obtained by setting $D = 30$. To evaluate the order parameters of each phase in the infinite D limit, we perform numerical calculations with different D 's, as shown in Fig. 6. Performing finite size scaling and extrapolating to infinite D , we find that the maximum value of M_+^{xy} in the XY-strip Neel phase (and the same for M_-^{xy} in the XY-Neel phase) vanishes as a power law of $D^{-0.24142}$. In contrast, the maximum value of M_+^z in the Ising stripe Neel phase approaches a finite number exponentially fast. This shows that when $\delta = 1$ the two XY phases in Fig. 5(a) are due to finite size effect (notice that M_+^{xy} decays very slowly with increasing D , so any finite D will give incorrect results) and will disappear in the phase diagram in the limit $D \rightarrow \infty$ (see Fig. 5(b)).

To illustrate that the XY phases will not disappear if $\delta \neq 1$, we perform a scaling for the order parameter M_+^y with D for $\delta = 0.9$. It turns out that M_+^y still varies as a power law of $D^{-3.803}$, when shifted by a constant M_0 (See Fig. 7). The fact that $M_0 \neq 0$ shows that M_+^y in the

XY-strip Neel phase (and the same for M_-^y in the XY Neel phase) is finite in the limit $D \rightarrow \infty$, and the phase diagram at finite D are qualitatively correct if $\delta \neq 1$.

2. Vanishing of the XY phases and $U(1)$ symmetry protected phase transitions

Physically, the disappearance of the two XY phases at $\delta = 1$ can be explained by quantum fluctuations.

When $\delta = 1$, the Hamiltonian (3) has an enhanced symmetry $[U(1) \times Z_2] \times \sigma$, where the $U(1)$ subgroup means rotation of the spins along z -axis, Z_2 is generated by a rotation of the spin for π around x -axis. Since the continuous symmetry $U(1)$ will never spontaneously break in 1D, if the XY phases exist, they will be quasi-long ranged ordered in x - y plane and gapless.

However, strong quantum fluctuations gap out these states and drive them into the SPT phases. From the semiclassical approach, the enhanced symmetry results in a larger degeneracy of the semiclassical ground states near $\lambda_{xy} \sim \lambda_z$. The enlarged degeneracy of the semiclassical ground states enhances the quantum fluctuations

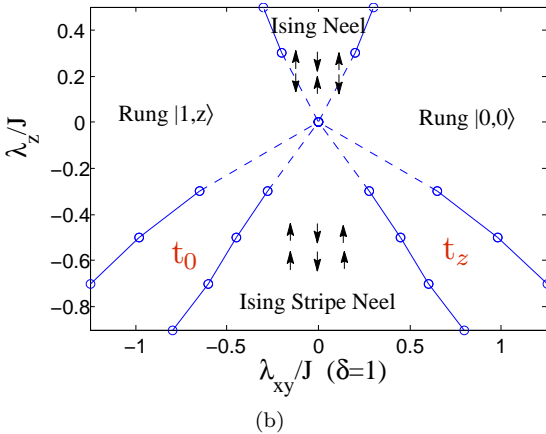
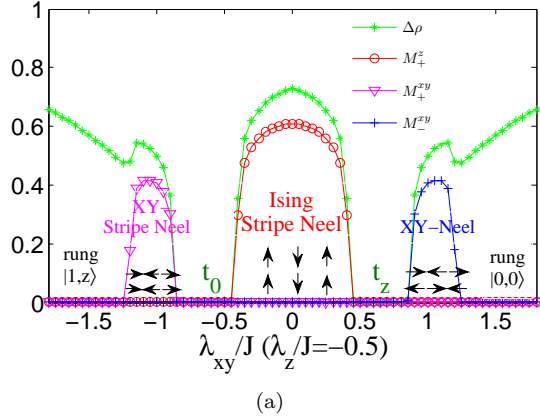


FIG. 5: (Color online) (a) Phase diagram obtained with $D = 30$ for $\delta = 1$, $\lambda_z = -0.5J$. The order parameters are defined as $M_+^z = |\langle S_1^z + S_2^z \rangle|$ and $M_+^{xy} = \sqrt{\langle S_1^x \pm S_2^x \rangle^2 + \langle S_1^y \pm S_2^y \rangle^2}$; (b) Phase diagram of $\delta = 1$ in the limit $D \rightarrow \infty$.

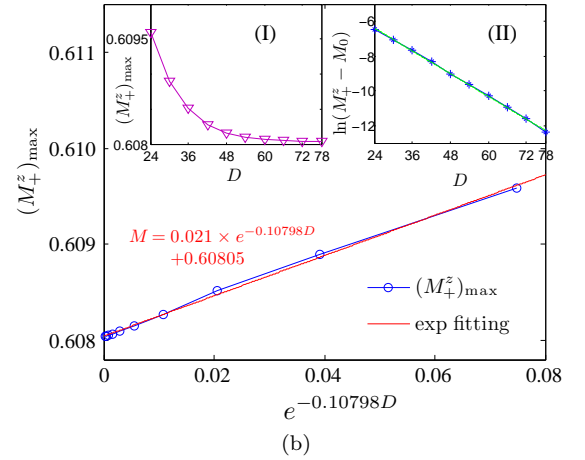
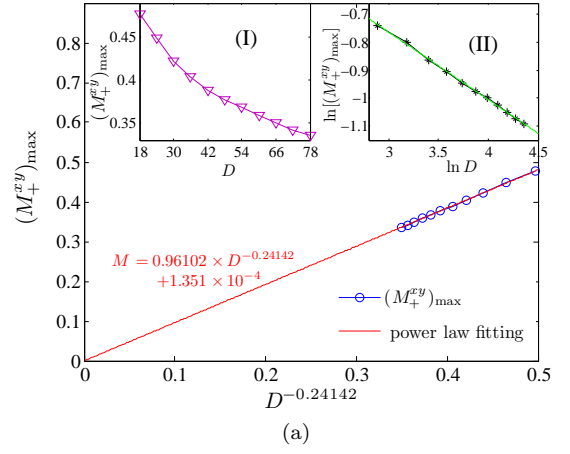


FIG. 6: (Color online) (a) Power law scaling of the maximum value of the order parameter M_+^{xy} with $\delta = 1$. The intercept shows that M_+^{xy} is vanishing in power law with the dimension D . Insert I shows the data of M_+^{xy} vs. dimension D . Insert II is a log-log fit of the data; (b) Exponential scaling of the maximum value of the order parameter M_+^z with $\delta = 1$. The intercept shows that M_+^z is finite at infinite D . Insert I shows the data of M_+^z vs. dimension D . Insert II is a log fit of the data.

and gap out all the states (except the states at the critical points). Consequently the XY phases disappear, and the nontrivial SPT phase t_0/t_z touches the trivial phase rung- $|1, z\rangle$ /rung- $|0, 0\rangle$ directly. That is to say, the direct transition between t_0/t_z and rung- $|1, z\rangle$ /rung- $|0, 0\rangle$ is protected by the continuous $U(1)$ symmetry.

Notice that similar situations also happen in $S = 1$ chains,¹ where the Haldane phase and the trivial phase (in analogy to the rung-phases) are separated by a Z_2 symmetry breaking phase when the system does not have a continuous symmetry [such as $U(1)$ spin rotational symmetry].

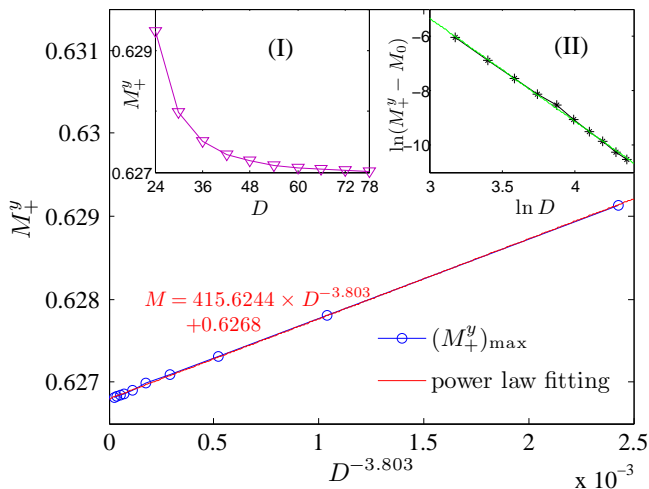


FIG. 7: (Color online) Power law scaling of the maximum value of the order parameter M_+^y with $\delta = 0.9$. The intercept shows that M_+^y is finite at infinite D . Insert (I) shows the data of M_+^y VS. dimension D . Insert (II) is a log-log fitting of the data.

IV. PHYSICAL REALIZATION AND QUANTUM SIMULATION

Here we propose possible realizations of the SPT phases in two-legged ladder Mott systems.²⁶ The Hamiltonian (3) can be considered as two Heisenberg chains coupled with magnetic dipole-dipole interaction and exchange interaction $H_T = \sum_i [\eta(\mathbf{S}_{1,i} \cdot \mathbf{S}_{2,i}) + \gamma(\mathbf{S}_{1,i} \cdot \mathbf{S}_{2,i} - 3S_{1,i}^z S_{2,i}^z)]$ with $\lambda_z = \eta - 2\gamma$ and $\lambda_{xy} = \eta + \gamma$. However, in real materials, the magnetic dipole-dipole interaction is too weak to support the SPT phases. On the other hand, axial anisotropy interaction $D_z(S_1^z + S_2^z)^2 = 2D_z(S_1^z S_2^z + 1)$ can yield the Hamiltonian (3) by $H_T = \sum_i [\eta(\mathbf{S}_{1,i} \cdot \mathbf{S}_{2,i}) + D_z(S_{1,i}^z + S_{2,i}^z)^2]$ with $\lambda_z = 2D_z + \eta$, $\lambda_{xy} = \eta$. Note that a weak effective spin-1 axial anisotropy term exists in the material $(\text{C}_5\text{H}_{12}\text{N})_2\text{CuBr}_4$.²⁷ If this term is negative and is strong enough in some material, then the t_z phase will be realized.

On the other hand, due to the nearest-neighbor-only interactions, it is tempting to consider the possibility of simulating these Hamiltonians in a non-condensed-matter setting. Here we provide a proof-of-principle implementation scheme for the Hamiltonians for the t_0 phase (1) and for the t_z phase (2) based on coupled-harmonic-oscillator array. Here we only consider the isotropic case with $\delta = 1$. Note that it is also possible to implement the more general anisotropic cases with additional Raman lasers along the ladder. Our scheme may be extended to systems including solid-spins interacting with arrays of coupled transmission line resonators, or ions in a Coulomb crystal. As a concrete example, we illustrate the scheme using a coupled-QED-cavity ladder (see Fig. 8(a)), where the quantized cavity fields couple to their nearest neighbors in the longitudinal (L) and

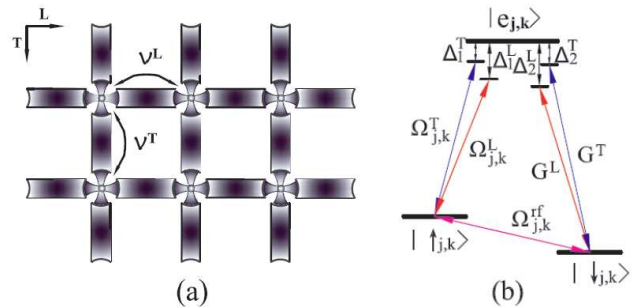


FIG. 8: (Color online) (a) Illustration of the coupled-cavity ladder. A single atom is held at the intersection of two cavity modes that are coupled across both the longitudinal (L) and the transverse (T) directions, with coupling rates v^L and v^T , respectively. (b) Schematic of the coupling scheme for the atom inside the cavity. The external lasers are applied perpendicularly to the plane of the ladder. The subscripts j, k of the parameters indicate the atom is on the j th site transversally and k th site longitudinally.

the transverse (T) directions via photon hopping.²⁸ The spin degrees of freedom on each site are encoded in the internal states of a single atom trapped inside the cavity.

In Fig. 8(b), we show the coupling scheme for a minimal model with three internal states, with $(|\uparrow_{j,k}\rangle, |\downarrow_{j,k}\rangle)$ corresponding to hyperfine states in the ground state manifold and $|e_{j,k}\rangle$ corresponding to an electronically excited state. Two far-detuned external laser fields with Rabi frequencies $\Omega_{j,k}^\mu = \Omega^\mu e^{i\theta_{j,k}^\mu}$ ($\mu = L, T$) couple $|\uparrow_{j,k}\rangle$ and $|e_{j,k}\rangle$, while two far-detuned cavity modes with Rabi frequencies G^μ couple $|e_{j,k}\rangle$ and $|\downarrow_{j,k}\rangle$, with all the detunings satisfying $|\Delta_2^L - \Delta_2^T|, |\Delta_1^L - \Delta_1^T|, |\Delta_1^\mu|, |\Delta_2^\mu| \gg G^\mu, \Omega^\mu, |\Delta_2^\mu - \Delta_1^\mu|$. Hence, we have two independent Raman paths in the longitudinal and in the transverse directions, and a virtually populated excited state $|e_{j,k}\rangle$. Finally, the hyperfine states are coupled using a resonant radio-frequency (r.f.) dressing field with Rabi frequency $\Omega_{j,k}^{\text{rf}} = \Omega^{\text{rf}} e^{i\varphi_{j,k}}$. One can show that all the cavity modes are virtually excited under the condition $|\Delta_2^\mu - \Delta_1^\mu| \sim \Omega^{\text{rf}} \gg g^\mu/\sqrt{2N}, v^\mu$, where $g^\mu = G^\mu \Omega^\mu (\Delta_1^\mu + \Delta_2^\mu)/2\Delta_1^\mu \Delta_2^\mu$, v^μ is the coupling rate between cavities along the direction μ , and N is the number of sites in the longitudinal direction.²⁹ After adiabatic elimination of the excited states and the cavity modes, the resulting effective Hamiltonian gives rise to effective spin-spin interactions between the neighboring sites, with the pseudo-spins in the effective Hamiltonian given by the superpositions of the hyperfine states: $|\uparrow'_{j,k}\rangle = (e^{i\varphi_{j,k}}|\uparrow_{j,k}\rangle + |\downarrow_{j,k}\rangle)/\sqrt{2}$, $|\downarrow'_{j,k}\rangle = (-|\uparrow_{j,k}\rangle + e^{-i\varphi_{j,k}}|\downarrow_{j,k}\rangle)/\sqrt{2}$.

Depending on the magnitude and the relative phases of the coupling fields, the effective Hamiltonian can support either the t_0 phase or the t_z phase. In particular, with $\Omega^{\text{rf}} \sim 0.75|\Delta_2^\mu - \Delta_1^\mu|$ and $|\theta_{j,k+1}^L - \theta_{j,k}^L| = \pi$, we get the Hamiltonian for the t_0 phase when $\theta_{j,k}^T = \varphi_{j,k} = 0$

for arbitrary j, k ; and we get the Hamiltonian for the t_z phase when $|\theta_{1,k}^T - \theta_{2,k}^T| = |\varphi_{1,k} - \varphi_{2,k}| = \pi$ and $\varphi_{j,k} = \varphi_{j,k+1}$ for arbitrary j, k . These conditions can be achieved by modulating the relative phases of the external coupling fields so that they are either 0 or π between neighboring sites. The interaction rates J and λ in Hamiltonian (1,2) are given as $J \sim 1.14 (g^L)^2 v^L / (\Omega^{\text{rf}})^2$, $\lambda = -1.14 (g^T)^2 v^T / (\Omega^{\text{rf}})^2$. For typical experimental parameters³⁰: $\Omega^\mu \sim 100\text{MHz}$, $G^\mu \sim 100\text{MHz}$, $|\Delta_i^\mu| \sim 1\text{GHz}$ ($i = 1, 2$), $v^\mu \sim 10\text{MHz}$, $\Omega^{\text{rf}} \sim 100\text{MHz}$, we have $J \sim 0.11\text{MHz}$, with the magnitude of λ/J widely tunable by adjusting the ratio between Ω^L and Ω^T .

The single-site addressability of the atoms in the cavity ladder allows much freedom in probing the properties of the system. For the SPT phases in which we are interested, we need to measure the response of the edge states to the magnetic field. As the pseudo-spins are related to the hyperfine states via a rotation, we may implement an effective magnetic field on the pseudo-spins by imposing the appropriately rotated operations on the edge states. For instance, to apply an effective magnetic field in the z -direction, we need to apply a σ_x rotation on the hyperfine states (assuming $\varphi_{j,k} = 0$), which can be achieved for example by adding a resonant r.f. field between the hyperfine states, with the effective Rabi frequency corresponding to the magnitude of the effective magnetic field. To probe the response of the edge states to the effective field, we may measure the polarization of the ground state of the system. Alternatively, as the effective magnetic field may induce an energy splitting between the spin states, we can measure the existence of energy splitting as a response of the SPT phases to the external field. As an example, for the t_z phase under an effective magnetic field along z , we need to implement the following steps on the two edge sites at one end of the open boundaries: (i) adiabatically turn on resonant r.f. fields between the hyperfine states so that the degeneracy of the edge states is lifted and an energy splitting appears between $|\uparrow'_{\text{edge}}\rangle$ and $|\downarrow'_{\text{edge}}\rangle$; (ii) in the presence of the effective magnetic field, apply an effective resonant coupling fields between the pseudo-spins, which corresponds to two-photon detuned Raman fields between the hyperfine states with the Stark shifts equal to the Rabi-frequency of the effective resonant coupling fields between the pseudo-spins; (iii) after some time of evolution, rapidly turn off all the coupling fields, then apply a $\pi/2$ -pulse on the hyperfine states, so that pseudo-spin population is projected onto that of the hyperfine states; (iv) the population of the hyperfine state can be probed for example by high-fidelity hyperfine state readout technique based on cavity-enhanced fluorescence.³¹ If the edge states are responsive to the effective magnetic field, one will observe Rabi-oscillations in the measured fluorescence. Measuring the magnetic field response in all three spatial directions will allow us to establish the signature of the t_z phase.

V. CONCLUSION AND ACKNOWLEDGEMENT

In summary, we have studied nontrivial quantum phases t_0 (the Haldane phase) and t_z (a new SPT phase different from the Haldane phase) protected by $D_2 \times \sigma$ symmetry in a spin-1/2 ladder model. The model has simple two-body interactions and a rich phase diagram. We then provided a semiclassical understanding of the physical properties of the SPT phases, and discussed the general principles for the search of these novel phases. Finally, we have proposed a proof-of-principle quantum simulation scheme of nontrivial SPT phases in cold atom systems.

ZXL would like to thank Fa Wang, Xie Chen, Tian-Heng Han and Salvatore R. Manmana for helpful discussions. This work is supported by NFRP (2011CB921200, 2011CBA00200), NNSF (60921091), NSFC (11105134, 11105135), the Fundamental Research Funds for the Central Universities (WK2470000001, WK2470000004, WK2470000006). XGW is supported by NSF DMR-1005541 and NSFC 11074140.

Appendix A: Constructing the Hamiltonians with SPT phases

In this Appendix, we demonstrate the method²¹ by which we obtain the Hamiltonian H_0 , H_x , H_y and H_z in the main text. The procedure contains three steps: (i) construct a matrix product state (MPS) wave function with given edge states which are described by the projective representations; (ii) construct the parent Hamiltonian for the MPS using projection operators; (iii) simplify the parent Hamiltonian by adiabatic deformations. In the first step, we need to know the projective and linear representations of the symmetry group, together with the Clebsch-Gordan (CG) coefficients. In the following, we will first present necessary information and then discuss the construction of the Hamiltonian step-by-step.

The four projective representations of $D_2 \times \sigma$ corresponding to the t_0, t_x, t_y, t_z phases are given in Tab. II (we only provide the representation matrices for the generators), and the eight linear representations are listed in Tab. III.

TABLE II: Four nontrivial SPT phases in $S = 1/2$ spin ladders respecting $D_2 \times \sigma$ symmetry.

	$M(R_z)$	$M(R_x)$	$M(\sigma)$	active operators
$E_3 (t_0)$	$i\sigma_z$	σ_x	I	(S_+^x, S_+^y, S_+^z)
$E_5 (t_x)$	$i\sigma_z$	σ_x	$i\sigma_x$	(S_+^x, S_-^y, S_-^z)
$E_6 (t_z)$	$i\sigma_z$	$i\sigma_x$	σ_z	(S_-^x, S_-^y, S_+^z)
$E_7 (t_y)$	$i\sigma_z$	$i\sigma_x$	$i\sigma_y$	(S_-^x, S_+^y, S_-^z)

TABLE III: Linear representations of $D_2 \times \sigma$. The four bases are defined as $|0, 0\rangle = \frac{1}{\sqrt{2}}(|\uparrow_1\downarrow_2\rangle - |\downarrow_1\uparrow_2\rangle)$, $|1, x\rangle = \frac{1}{\sqrt{2}}(|\downarrow_1\downarrow_2\rangle - |\uparrow_1\uparrow_2\rangle)$, $|1, y\rangle = \frac{i}{\sqrt{2}}(|\downarrow_1\downarrow_2\rangle + |\uparrow_1\uparrow_2\rangle)$, and $|1, z\rangle = \frac{1}{\sqrt{2}}(|\uparrow_1\downarrow_2\rangle + |\downarrow_1\uparrow_2\rangle)$, where the subscripts 1, 2 label the different spins on the same rung. The operator $S_+^m = S_1^m + S_2^m$ ($m = x, y, z$) is even under inter-chain reflection, and $S_-^m = S_1^m - S_2^m$ is odd under the reflection.

	R_z	R_x	σ	bases	operators
A_g	1	1	1		
B_{1g}	1	-1	1	$ 1, z\rangle$	S_+^z
B_{2g}	-1	-1	1	$ 1, y\rangle$	S_+^y
B_{3g}	-1	1	1	$ 1, x\rangle$	S_+^x
A_u	1	1	-1	$ 0, 0\rangle$	
B_{1u}	1	-1	-1		S_-^z
B_{2u}	-1	-1	-1		S_-^y
B_{3u}	-1	1	-1		S_-^x

The Hilbert space of the direct product of two projective representations can be reduced to a direct sum of linear representations. The CG coefficients (we assume that all the CG coefficients are real numbers) are :

$$E_3 \otimes E_3 = A_g \oplus B_{1g} \oplus B_{2g} \oplus B_{3g}, \quad C^{A_g} = \sigma_x, \quad C^{B_{1g}} = i\sigma_y, \quad C^{B_{2g}} = \sigma_z, \quad C^{B_{3g}} = I; \quad (\text{A1})$$

$$E_5 \otimes E_5 = B_{1g} \oplus B_{2g} \oplus A_u \oplus B_{3u}, \quad C^{A_u} = \sigma_x, \quad C^{B_{3u}} = I, \quad C^{B_{1g}} = i\sigma_y, \quad C^{B_{2g}} = \sigma_z; \quad (\text{A2})$$

$$E_6 \otimes E_6 = B_{2g} \oplus B_{3g} \oplus A_u \oplus B_{1u}, \quad C^{A_u} = i\sigma_y, \quad C^{B_{1u}} = \sigma_x, \quad C^{B_{2g}} = I, \quad C^{B_{3g}} = \sigma_z; \quad (\text{A3})$$

$$E_7 \otimes E_7 = A_g \oplus B_{2g} \oplus B_{1u} \oplus B_{3u}, \quad C^{A_g} = i\sigma_y, \quad C^{B_{2g}} = I, \quad C^{B_{1u}} = \sigma_x, \quad C^{B_{3u}} = \sigma_z, \quad (\text{A4})$$

where $|m\rangle = C_{\alpha\beta}^m |\alpha\rangle |\beta\rangle$, $|m\rangle$ is the basis of a linear representation and $|\alpha\rangle, |\beta\rangle$ are the bases of two projective representations.

In the following, we will illustrate the method to obtain the Hamiltonian of the t_0 phase as an example.

The first step is obtaining the MPS. From Tab. II, the edge states of the t_0 phase are described by the E_3 projective representation. In an ideal MPS, every rung is represented by a direct product of two E_3 projective representations, which can be reduced to four linear representations, $E_3 \otimes E_3 = A_g \oplus B_{1g} \oplus B_{2g} \oplus B_{3g}$. From Tab. III, B_{1g}, B_{2g}, B_{3g} correspond to the bases $|1, z\rangle, |1, y\rangle, |1, x\rangle$ respectively. The basis A_g (or $|0, 0\rangle$) is absent on every rung in the MPS state. Thus, the support space for the ideal MPS is the Hilbert subspace $\otimes_i (|1, z\rangle \oplus |1, y\rangle \oplus |1, x\rangle)_i$, where i is the index of rung. From the CG coefficients (A1), we can write such an ideal MPS which is invariant (up to a phase) under the symmetry group:

$$|\psi\rangle = \sum_{\{m_1, \dots, m_N\}} \text{Tr}(A^{m_1} \dots A^{m_N}) |m_1 \dots m_N\rangle,$$

with $A^m = e^{i\theta_m} B C^m$. Here B is the CG coefficients of decomposing the product representations $E_3 \otimes E_3$ into a 1D representation (here we choose $B = C^{A_g}$), and $e^{i\theta_m}$ can be absorbed into the spin bases. Now we have,

$$A^{|1,x\rangle} = \sigma_x, \quad A^{|1,y\rangle} = \sigma_y, \quad A^{|1,z\rangle} = \sigma_z, \quad (\text{A5})$$

The second step is constructing the parent Hamiltonian, which is a sum of projectors. Each projector is a projection onto the ground state subspace of two neighboring rungs. Assuming the orthonormal bases for the MPS state of two neighboring rungs $i, i+1$ are $\psi_1, \psi_2, \psi_3, \psi_4$, then the projector is $P_{i,i+1} = -(\sum_{a=1}^4 |\psi_a\rangle \langle \psi_a|)_{i,i+1}$ and the resultant parent Hamiltonian $H_{0\text{ex}} = \sum_i P_{i,i+1}$ is given as,

$$H_{0\text{ex}} = J \sum_i \left[\frac{5}{12} (\mathbf{S}_{1,i} + \mathbf{S}_{2,i}) \cdot (\mathbf{S}_{1,i+1} + \mathbf{S}_{2,i+1}) - \frac{2}{3} \mathbf{S}_{1,i} \cdot \mathbf{S}_{2,i} - \frac{2}{3} (\mathbf{S}_{1,i} \cdot \mathbf{S}_{2,i}) (\mathbf{S}_{1,i+1} \cdot \mathbf{S}_{2,i+1}) \right. \\ \left. + \frac{1}{3} (\mathbf{S}_{1,i} \cdot \mathbf{S}_{1,i+1}) (\mathbf{S}_{2,i} \cdot \mathbf{S}_{2,i+1}) + \frac{1}{3} (\mathbf{S}_{1,i} \cdot \mathbf{S}_{2,i+1}) (\mathbf{S}_{2,i} \cdot \mathbf{S}_{1,i+1}) \right]. \quad (\text{A6})$$

The final step is deforming the Hamiltonian. It can be shown that only the first two terms in (A6) are important.

To see this, we introduce the parameter d ,

$$H = J \sum_i \left[\frac{5}{12} (\mathbf{S}_{1,i} \cdot \mathbf{S}_{1,i+1} + \mathbf{S}_{2,i} \cdot \mathbf{S}_{1,i+1}) - \frac{2}{3} \mathbf{S}_{1,i} \cdot \mathbf{S}_{2,i} \right] + d \sum_i \left[\frac{5}{12} (\mathbf{S}_{1,i} \cdot \mathbf{S}_{2,i+1} + \mathbf{S}_{2,i} \cdot \mathbf{S}_{1,i+1}) - \frac{2}{3} (\mathbf{S}_{1,i} \cdot \mathbf{S}_{2,i}) (\mathbf{S}_{1,i+1} \cdot \mathbf{S}_{2,i+1}) + \frac{1}{3} (\mathbf{S}_{1,i} \cdot \mathbf{S}_{1,i+1}) (\mathbf{S}_{2,i} \cdot \mathbf{S}_{2,i+1}) + \frac{1}{3} (\mathbf{S}_{1,i} \cdot \mathbf{S}_{2,i+1}) (\mathbf{S}_{2,i} \cdot \mathbf{S}_{1,i+1}) \right]. \quad (\text{A7})$$

Note that when $d/J = 1$, (A7) is the same as (A6). Now we study the ground state energy and entanglement spectrum (through time-evolving block decimation method) to see if there is a phase transition when d is varied.

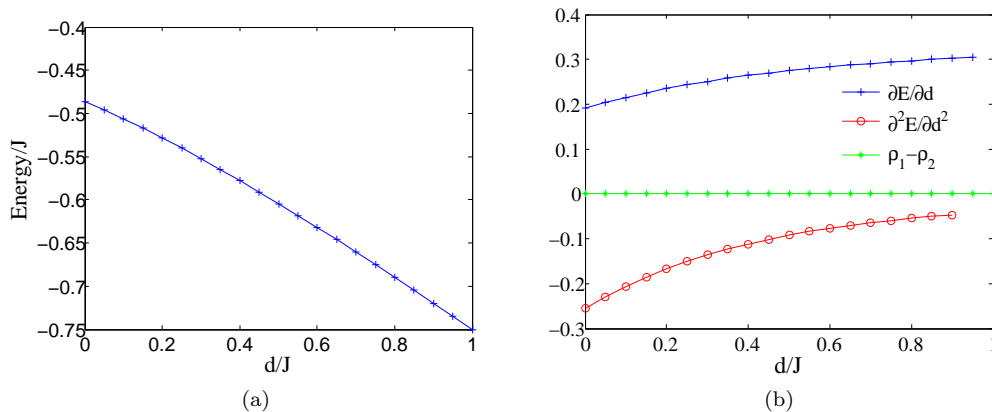


FIG. 9: (Color online) (a) Energy VS. d/J . (b) The derivatives of the energy curve with respect to the parameter d and the information of entanglement spectrum.

Fig. 9 shows that the energy is a smooth function of parameter $d/J \in [0, 1]$. Furthermore, the entanglement spectrum remains degenerate in $d/J \in [0, 1]$. Thus we only need nearest-neighbor exchanges to realize the Haldane (t_0) phase, which leads to the Hamiltonian H_0 in the main text.

The active operators in Tab. II are obtained as the following. In the Hilbert space spanned by the two-fold degenerate edge states, only the Pauli matrices ($\sigma_x, \sigma_y, \sigma_z$) can lift the degeneracy. But these operators are not physical quantities. We need to find physical spin operators which vary in the same way as these Pauli matrices under the symmetry group. In other words, we require that the active operators form the same linear representations as ($\sigma_x, \sigma_y, \sigma_z$), respectively. For example, in the E_3 projective representation, σ_x varies as

$$\begin{aligned} M(R_z)^\dagger \sigma_x M(R_z) &= -\sigma_x, \\ M(R_x)^\dagger \sigma_x M(R_x) &= \sigma_x, \\ M(\sigma)^\dagger \sigma_x M(\sigma) &= \sigma_x. \end{aligned}$$

On the other hand, from Tab. III,

$$\begin{aligned} R_z^\dagger S_+^x R_z &= -S_+^x, \\ R_x^\dagger S_+^x R_x &= S_+^x, \\ \sigma^\dagger S_+^x \sigma &= S_+^x. \end{aligned}$$

We find that S_+^x and σ_x belong to the same linear representation B_{3g} under the symmetry operation. This means that in the low energy limit (i.e. in the ground state subspace), these two operators have similar behavior. So we can identify S_+^x as an active operator. Similarly, the operators S_+^y and S_+^z are active operators corresponding to σ_y and σ_z respectively.

Similar to (A6), we can construct the exactly solvable Hamiltonian H_{zex} of the t_z phase. It is the same as (A6) except that every $\mathbf{A} \cdot \mathbf{B}$ term is replaced by $A_z B_z - A_x B_x - A_y B_y$. This Hamiltonian can be simplified into the form of H_z [Eqn.(3) of the main text] without any phase transition (H_x and H_y are obtained similarly).

The active operators in t_z phase can be easily obtained: S_-^x, S_-^y, S_+^z . Notice that S_+^x, S_+^y are not active operators, meaning that the edge states in the ground state will not respond to the uniform magnetic in x and y directions. To check this result, we perform a finite-size exact diagonalization of the solvable model H_{zex} . As shown in Fig.10, only

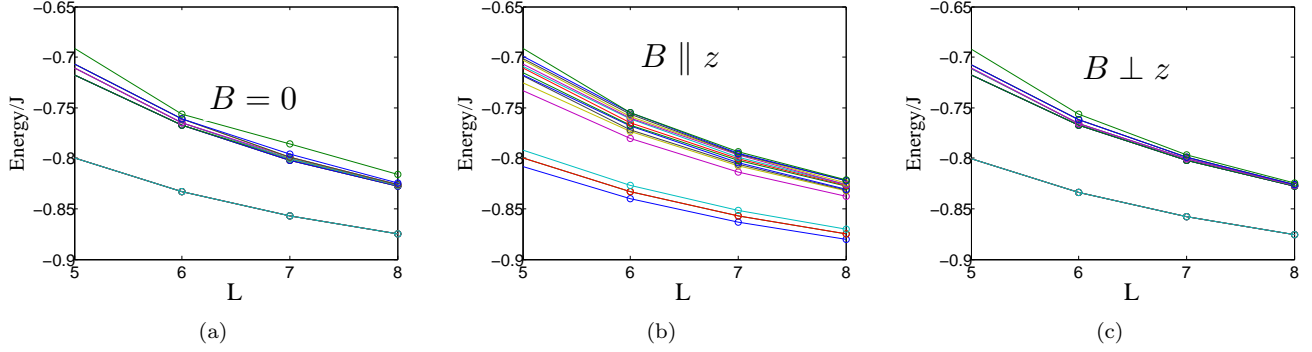


FIG. 10: The spectrum of the ground states and some excited states in t_z phase, L is the length of the ladder. (a) $B = 0$, the ground states are 4-fold degenerate; (b) $B \parallel z$, the degeneracy of ground states is split; (c) $B \perp z$, the ground states remains degenerate.

the magnetic field along z direction can split the ground state degeneracy. These properties are valid in the whole t_z phase in thermodynamic limit. This verifies the conclusion that only S^z_+ is the active operator.

This interesting result indicates that we can distinguish t_z from t_0 by the response to magnetic fields. In t_0 phase, arbitrarily small magnetic field can split the degeneracy of the ground states, showing that the edge states carry free magnetic moments. According to Curie's law, the magnetic susceptibility will diverge at low temperature. But in t_z phase, the edge states only carry magnetic moment in z direction, so the magnetic susceptibility within the XY plane does not diverge at low temperature, but it does diverge if the magnetic field is along z direction. These results are also verified numerically, see Fig. 11. The behavior of low-temperature magnetic susceptibility is measurable, which

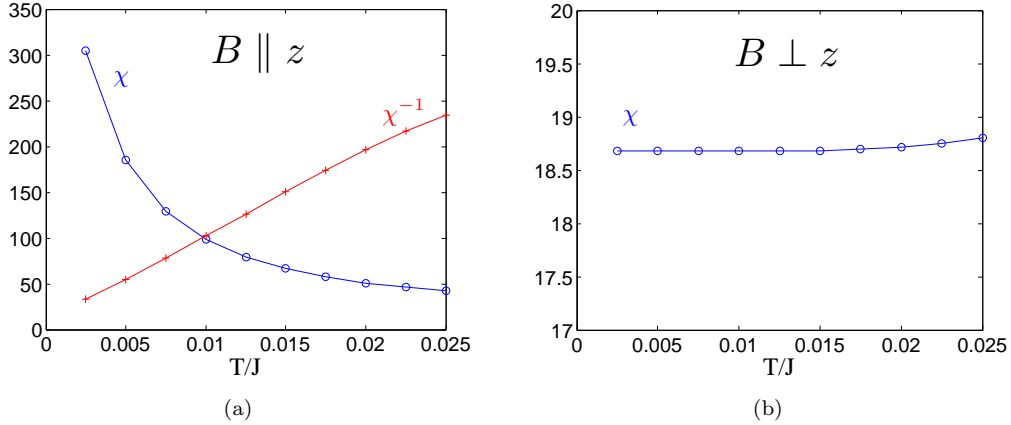


FIG. 11: The susceptibility in t_z phase. (a) χ diverges at $T = 0$ if $B \parallel z$; (b) χ is finite at $T = 0$ if $B \perp z$.

allows us to distinguish different SPT phases experimentally.

Appendix B: Implementing the ladder Hamiltonian

In this Appendix, we discuss in more detail the implementation scheme for the Hamiltonian with SPT phases. To keep our discussion general, we consider a two-dimensional (2D) coupled-harmonic-oscillator-array. Later, we will relate this general scheme to the specific example of a cavity-ladder as in the main text.

Consider a 2D array, on each site of the array, two independent harmonic oscillators exist and couple with

those on the neighboring sites via energy tunneling. We label these harmonic oscillators as L (longitudinal) and T (transverse), and assume that oscillators only couple with those having the same label on the neighboring sites along the direction specified by their labels. This can be achieved by requiring the frequency difference between different types of oscillators (L and T) to be sufficiently large, and by setting up specific coupling schemes between neighboring sites. The Hamiltonian for this 2D coupled-harmonic-oscillator-array can be written

as ($\hbar=1$)

$$H_1 = \sum_{j,k} \sum_{\mu=L,T} (v^L a_{j,k}^{L+} a_{j,k+1}^L + v^T a_{j,k}^{T+} a_{j+1,k}^T + H.c.), \quad (\text{B1})$$

where $a_{j,k}^L$ ($a_{j,k}^T$) is the annihilation operator for the harmonic oscillator labeled L (T) on the j th site transversally and the k th site longitudinally. The coupling strength along the longitudinal (transverse) direction is given by v_L (v_T).

The harmonic oscillators on each site interact with a two-level system $\{|\uparrow_{j,k}\rangle, |\downarrow_{j,k}\rangle\}$, and the coupling rates are $g_{j,k}^L = g^L e^{i\theta_{j,k}^L t}$ and $g_{j,k}^T = g^T e^{i\theta_{j,k}^T t}$, respectively. This is illustrated in Fig. 12. The interaction Hamiltonian is

$$H_2 = \sum_{j,k} \sum_{\mu=L,T} (g_{j,k}^\mu e^{i\Delta^\mu t} a_{j,k}^\mu S_{j,k}^+ + H.c.), \quad (\text{B2})$$

where $S_{j,k}^+ = |\uparrow_{j,k}\rangle\langle\downarrow_{j,k}|$, and Δ^L (Δ^T) denotes the detuning of the corresponding harmonic oscillator mode (see Fig. 12). Finally, the two-level system on each site is coupled by a resonant dressing field, with the Hamiltonian

$$H_3 = \sum_{j,k} \sum_{\mu=L,T} (\Omega_{j,k}^{\text{rf}} S_{j,k}^+ + H.c.), \quad (\text{B3})$$

Before doing so, let us first introduce the following transformations

$$a_{j,k}^\mu = \frac{1}{\sqrt{MN}} \sum_{m,n} \exp[-i(\frac{2\pi jm}{M} + \frac{2\pi kn}{N})] a_{m,n}^{\mu}, \quad (\text{B4})$$

$$|\uparrow'_{j,k}\rangle = \frac{1}{\sqrt{2}} (e^{i\varphi_{j,k}} |\uparrow_{j,k}\rangle + |\downarrow_{j,k}\rangle), \quad (\text{B5})$$

$$|\downarrow'_{j,k}\rangle = \frac{1}{\sqrt{2}} (-|\uparrow_{j,k}\rangle + e^{-i\varphi_{j,k}} |\downarrow_{j,k}\rangle), \quad (\text{B6})$$

where M and N are the total number of sites in the longitudinal and transverse direction, respectively. While Eq. (B4) diagonalizes H_1 , (B5) and (B6) define the pseudo-spin basis $\{|\uparrow'_{j,k}\rangle, |\downarrow'_{j,k}\rangle\}$.

With these, the Hamiltonians become

$$H'_1 = \sum_{m,n} \sum_{\mu=L,T} \omega_{m,n}^\mu a_{m,n}^{\mu+} a_{m,n}^{\mu}, \quad (\text{B7})$$

$$H'_2 = \sum_{j,k} \sum_{\mu=L,T} [\frac{g_{j,k}^\mu}{\sqrt{MN}} \sum_{m,n} \exp^{-i(\frac{2\pi jm}{M} + \frac{2\pi kn}{N})} a_{m,n}^{\mu} e^{i\Delta^\mu t} (e^{-i\varphi_{j,k}} \frac{1}{\sqrt{2}} S_{j,k}^{\prime z} + e^{-i2\varphi_{j,k}} \frac{1}{2} S_{j,k}^{\prime+} - \frac{1}{2} S_{j,k}^{\prime-}) + H.c.], \quad (\text{B8})$$

$$H'_3 = \sum_{j,k} \sum_{\mu=L,T} \sqrt{2} \Omega_{j,k}^{\text{rf}} S_{j,k}^{\prime z}, \quad (\text{B9})$$

where $\omega_{m,n}^L = 2v^L \cos(\frac{2\pi n}{N})$, $\omega_{m,n}^T = 2v^T \cos(\frac{2\pi m}{M})$. The pseudo-spin operators are defined through the pseudo-spin basis states: $S_{j,k}^{\prime+} = |\uparrow'_{j,k}\rangle\langle\downarrow'_{j,k}|$, and $S_{j,k}^{\prime-} = |\downarrow'_{j,k}\rangle\langle\uparrow'_{j,k}|$.

where $\Omega_{j,k}^{\text{rf}} = \Omega^{\text{rf}} e^{i\varphi_{j,k}}$ is the Rabi frequency.

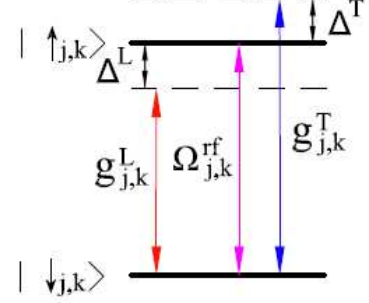


FIG. 12: Schematic for the coupling scheme of the two-level system on each site.

Starting from the full Hamiltonian $H = H_1 + H_2 + H_3$, we will eventually adiabatically eliminate the harmonic oscillator modes and derive an effective Hamiltonian for the dynamics of the coupled two-level systems throughout the array.

We now go to the rotating frame via the transformation $R = \exp[-i(H'_1 + H'_3)t]$

$$\begin{aligned}
H'' &= R^\dagger \left(\sum_i H'_i \right) R - iR^\dagger \frac{dR}{dt} \\
&= \sum_{j,k} \sum_{\mu=L,T} \left\{ \frac{g_{j,k}^\mu}{\sqrt{MN}} \sum_{m,n} e^{-i(\frac{2\pi jm}{M} + \frac{2\pi kn}{N})} a_{m,n}^\mu e^{i(\Delta^\mu - \omega_{m,n})t} [e^{-i\varphi_{j,k}} \frac{1}{\sqrt{2}} S'_{j,k}{}^Z + e^{-i(2\varphi_{j,k} - \sqrt{2}\Omega^{\text{rf}}t)} \frac{1}{2} S'_{j,k}{}^+ - \frac{1}{2} S'_{j,k}{}^- e^{-i\sqrt{2}\Omega^{\text{rf}}t}] \right. \\
&\quad \left. + H.c. \right\}. \tag{B10}
\end{aligned}$$

Under the condition $|\Delta^T - \Delta^L| \sim |\Delta^\mu| \sim |\Delta^\mu \pm \sqrt{2}\Omega^{\text{rf}}| \sim \sqrt{2}\Omega^{\text{rf}} \gg \frac{g^\mu}{\sqrt{MN}}, \omega_{m,n}^\mu$, the oscillator modes are virtually populated. We may adiabatically eliminate $a_{j,k}^\mu$ and describe the dynamics of the system using the resultant effective Hamiltonian^{29?}

$$\begin{aligned}
H_{\text{eff}} &= \sum_{j,k} \sum_{\mu=L,T} \sum_{m,n} \left\{ \frac{(g^\mu)^2}{MN} \left[\frac{1}{2} \frac{1}{\Delta^\mu - \omega_{m,n}^\mu} (S'_{j,k}{}^z)^2 + \frac{1}{4} \frac{1}{\Delta^\mu - \omega_{m,n}^\mu + \sqrt{2}\Omega^{\text{rf}}} S'_{j,k}{}^+ S'_{j,k}{}^- + \frac{1}{4} \frac{1}{\Delta^\mu - \omega_{m,n}^\mu - \sqrt{2}\Omega^{\text{rf}}} S'_{j,k}{}^- S'_{j,k}{}^+ \right] \right. \\
&\quad + \sum_{j,k \neq j',k'} \left[\frac{\cos(\frac{2\pi(j-j')m}{M} + \frac{2\pi(k-k')n}{N}) + \varphi_{j,k} - \varphi_{j',k'} + \theta_{j',k'}^\mu - \theta_{j,k}^\mu}{\Delta^\mu - \omega_{m,n}^\mu} S'_{j,k}{}^z S'_{j',k'}{}^z \right. \\
&\quad + \frac{1}{4} \left(\frac{e^{-i(\frac{2\pi(j-j')m}{M} + \frac{2\pi(k-k')n}{N})} e^{-i[2(\varphi_{j,k} - \varphi_{j',k'}) + \theta_{j',k'}^\mu - \theta_{j,k}^\mu]}}{\Delta^\mu - \omega_{m,n}^\mu + \sqrt{2}\Omega^{\text{rf}}} + \frac{e^{i[\frac{2\pi(j-j')m}{M} + \frac{2\pi(k-k')n}{N}]} e^{i(\theta_{j',k'}^\mu - \theta_{j,k}^\mu)}}{\Delta^\mu - \omega_{m,n}^\mu - \sqrt{2}\Omega^{\text{rf}}} \right) S'_{j,k}{}^+ S'_{j',k'}{}^- \\
&\quad \left. + \frac{1}{4} \left(\frac{e^{-i(\frac{2\pi(j-j')m}{M} + \frac{2\pi(k-k')n}{N})} e^{-i(\theta_{j',k'}^\mu - \theta_{j,k}^\mu)}}{\Delta^\mu - \omega_{m,n}^\mu - \sqrt{2}\Omega^{\text{rf}}} + \frac{e^{i(\frac{2\pi(j-j')m}{M} + \frac{2\pi(k-k')n}{N})} e^{i[2(\varphi_{j,k} - \varphi_{j',k'}) + \theta_{j',k'}^\mu - \theta_{j,k}^\mu]}}{\Delta^\mu - \omega_{m,n}^\mu + \sqrt{2}\Omega^{\text{rf}}} \right) S'_{j,k}{}^- S'_{j',k'}{}^+ \right\}. \tag{B11}
\end{aligned}$$

Adopting the formulae: $\sum_n \cos(\frac{2\pi n}{N}) \equiv 0$, $\sum_n \cos^2(\frac{2\pi n}{N}) = \sum_n \cos(\frac{2\pi n}{N}) e^{\pm i\frac{2\pi n}{N}} \equiv \frac{N}{2}$, and keeping only on-site and nearest-neighbor interactions, we can further simplify the effective Hamiltonian

$$\begin{aligned}
H_{\text{eff}} &\simeq \sum_{j,k} \sum_{\mu=L,T} \left\{ \frac{(g^\mu)^2 \Delta^\mu}{2[(\Delta^\mu)^2 - 2(\Omega^{\text{rf}})^2]} (S'_{j,k})^2 - \frac{(g^\mu)^2 (\Omega^{\text{rf}})^2}{\Delta^\mu [(\Delta^\mu)^2 - 2(\Omega^{\text{rf}})^2]} (S'_{j,k}{}^z)^2 - \frac{(g^\mu)^2 \Omega^{\text{rf}}}{2\sqrt{2}[(\Delta^\mu)^2 - 2(\Omega^{\text{rf}})^2]} S'_{j,k}{}^z \right\} \\
&\quad - (-1)^{\frac{|\theta_{j,k+1}^L - \theta_{j,k}^L|}{\pi}} \sum_{j,k} (g^L)^2 \left\{ (-1)^{\frac{|\varphi_{j,k+1} - \varphi_{j,k}|}{\pi}} \frac{v^L}{(\Delta^L)^2} S'_{j,k}{}^z S'_{j,k+1}{}^z + \frac{v^L [(\Delta^L)^2 + 2(\Omega^{\text{rf}})^2]}{[(\Delta^L)^2 - 2(\Omega^{\text{rf}})^2]^2} (S'_{j,k}{}^x S'_{j,k+1}{}^x + S'_{j,k}{}^y S'_{j,k+1}{}^y) \right\} \\
&\quad - (-1)^{\frac{|\theta_{j+1,k}^T - \theta_{j,k}^T|}{\pi}} \sum_{j,k} (g^T)^2 \left\{ (-1)^{\frac{|\varphi_{j+1,k} - \varphi_{j,k}|}{\pi}} \frac{v^T}{(\Delta^T)^2} S'_{j,k}{}^z S'_{j+1,k}{}^z + \frac{v^T [(\Delta^T)^2 + 2(\Omega^{\text{rf}})^2]}{[(\Delta^T)^2 - 2(\Omega^{\text{rf}})^2]^2} (S'_{j,k}{}^x S'_{j+1,k}{}^x + S'_{j,k}{}^y S'_{j+1,k}{}^y) \right\}. \tag{B12}
\end{aligned}$$

While the first two terms on the first line in Eq. (B12) are constant and can be dropped, the third term is a Stark-shift in the pseudo-spin basis, and can be canceled via local optical elimination.³² This corresponds to applying a r.f. or Raman fields with appropriate magnitude and phase between the hyperfine states such that the effective Stark-shift is canceled. Then, under the condition $3(\Delta^\mu)^2 = 2(\Omega^{\text{rf}})^2$, we have

$$\begin{aligned}
H_{\text{eff}} &\simeq -(-1)^{\frac{|\theta_{j,k+1}^L - \theta_{j,k}^L|}{\pi}} \frac{3(g^L)^2 v^L}{2(\Omega^{\text{rf}})^2} \sum_{j,k} \left[(-1)^{\frac{|\varphi_{j,k+1} - \varphi_{j,k}|}{\pi}} S'_{j,k}{}^z S'_{j,k+1}{}^z + S'_{j,k}{}^x S'_{j,k+1}{}^x + S'_{j,k}{}^y S'_{j,k+1}{}^y \right] \\
&\quad - (-1)^{\frac{|\theta_{j+1,k}^T - \theta_{j,k}^T|}{\pi}} \frac{3(g^T)^2 v^T}{2(\Omega^{\text{rf}})^2} \sum_{j,k} \left[(-1)^{\frac{|\varphi_{j+1,k} - \varphi_{j,k}|}{\pi}} S'_{j,k}{}^z S'_{j+1,k}{}^z + S'_{j,k}{}^x S'_{j+1,k}{}^x + S'_{j,k}{}^y S'_{j+1,k}{}^y \right]. \tag{B13}
\end{aligned}$$

Eq. (B13) gives the most general form of the effective Hamiltonian using our setup. For the spin-ladder Hamiltonians we considered in the main text, we may take $M = 2$ so that $j = 1, 2$ in the summations. Then, depending on the magnitudes and the relative phases of the coupling fields, we have either the Hamiltonian for the t_0 phase (t_0 model) or the Hamiltonian for the t_z phase (t_z model). In particular, with $|\theta_{j,k+1}^L - \theta_{j,k}^L| = \pi$, $\theta_{j,k}^T = \varphi_{j,k} = 0$ for arbitrary

$\{j, k\}$, the Hamiltonian reduces to the t_0 model

$$H_0 = J \sum_{j=1}^2 \sum_k (S'_{j,k}{}^z S'_{j,k+1}{}^z + S'_{j,k}{}^x S'_{j,k+1}{}^x + S'_{j,k}{}^y S'_{j,k+1}{}^y) + \lambda \sum_k (S'_{1,k}{}^z S'_{2,k}{}^z + S'_{1,k}{}^x S'_{2,k}{}^x + S'_{1,k}{}^y S'_{2,k}{}^y), \quad (\text{B14})$$

where the interaction rate $J = \frac{3(g^L)^2 v^L}{2(\Omega^{\text{rf}})^2}$ and $\lambda = -\frac{3(g^T)^2 v^T}{2(\Omega^{\text{rf}})^2}$. On the other hand, when $|\theta_{j,k+1}^L - \theta_{j,k}^L| = |\theta_{1,k}^T - \theta_{2,k}^T| = \pi$, $|\varphi_{1,k} - \varphi_{2,k}| = \pi$ and $\varphi_{j,k} = \varphi_{j,k+1}$, the Hamiltonian reduces to the t_z model

$$H_z = J \sum_{j=1}^2 \sum_k (S'_{j,k}{}^z S'_{j,k+1}{}^z + S'_{j,k}{}^x S'_{j,k+1}{}^x + S'_{j,k}{}^y S'_{j,k+1}{}^y) + \lambda \sum_k (S'_{1,k}{}^z S'_{2,k}{}^z - S'_{1,k}{}^x S'_{2,k}{}^x - S'_{1,k}{}^y S'_{2,k}{}^y). \quad (\text{B15})$$

A straightforward example for the realization of the coupled-harmonic-oscillator-array is the coupled quantum electrodynamics (QED) cavity array, as shown in FIG. 5(a) in the main text. In such a system, atoms or solid spins interact with the quantized cavity fields, which couple to their neighboring ones across both the longitudinal and transverse directions via photon hopping.²⁸ The two-level system in our general model can be replaced by a three-level structure, with two low-lying hyperfine states and an electronically excited state. Correspondingly, the coupling $g_{j,k}^L$ ($g_{j,k}^T$) in the general model is replaced by a Raman path in the longitudinal (transverse) direction, with an external laser field and a cavity mode each contributing a leg in the Raman coupling. Note that due to the large difference in the two-photon

detuning of the Raman couplings, the two Raman paths are effectively independent. It is then straightforward to work out the correspondence: $g^\mu = \frac{G^\mu \Omega^\mu}{2} (\frac{1}{\Delta_1^\mu} + \frac{1}{\Delta_2^\mu})$, $|\Delta^\mu| = |\Delta_2^\mu - \Delta_1^\mu|$, where G^μ is the Rabi frequency for the atom-cavity coupling, Δ^μ is the detuning (c.f. Fig. 5 in the main text). Importantly, one may realize Hamiltonians of different SPT phases (t_0 or t_z) by adjusting the phases of the Rabi frequencies $\Omega_{j,k}^\mu$ and $\Omega_{j,k}^{\text{rf}}$. For typical experimental parameters³⁰: $\Omega^\mu \sim 100\text{MHz}$, $G^\mu \sim 100\text{MHz}$, $|\Delta_i^\mu| \sim 1\text{GHz}$ ($i = 1, 2$), $v^\mu \sim 10\text{MHz}$, $\Omega^{\text{rf}} \sim 100\text{MHz}$, we have $J \sim 0.15\text{MHz}$, with the magnitude of λ/J widely tunable by adjusting the ratio between Ω^L and Ω^T .

* Electronic address: zbyang@ustc.edu.cn

† Electronic address: wyz@ustc.edu.cn

‡ Electronic address: wen@dao.mit.edu

¹ Zheng-Cheng Gu, Xiao-Gang Wen, Phys. Rev. B **80**, 155131(2009).

² Xie Chen, Zheng-Cheng Gu, Xiao-Gang Wen, Phys. Rev. B **82**, 155138(2010).

³ F. Pollmann, A. M. Turner, E. Berg, and M. Oshikawa, arXiv:0909.4059 (2009); Phys. Rev. B **81**, 064439 (2010).

⁴ F. D. M. Haldane, Phys. Rev. Lett. **50**, 1153 (1983), Phys. Lett. **93**, 464 (1983); I. Affleck and F. D. M. Haldane, Phys. Rev. B **36**, 5291 (1987); I. Affleck, J. Phys.: Condens. Matter. **1**, 3047 (1989).

⁵ C. L. Kane and E. J. Mele, Phys. Rev. Lett. **95**, 226801 (2005), cond-mat/0411737.

⁶ B. A. Bernevig and S. C. Zhang, Phys. Rev. Lett. **96**, 106802 (2005), cond-mat/0504147.

⁷ C. L. Kane and E. J. Mele, Phys. Rev. Lett. **95**, 146802 (2005), cond-mat/0506581.

⁸ J. E. Moore and L. Balents, Phys. Rev. B **75**, 121306 (2007), cond-mat/0607314.

⁹ L. Fu, C. L. Kane, and E. J. Mele, Phys. Rev. Lett. **98**, 106803 (2007), cond-mat/0607699.

¹⁰ X.-L. Qi, T. L. Hughes, and S.-C. Zhang, Phys. Rev. B **78**, 195424 (2008), arXiv:0802.3537.

¹¹ M. Hagiwara, K. Katsumata, Ian Affleck, B. I. Halperin, and J. P. Renard, Phys. Rev. Lett **65**, 3181 (1990).

¹² Steven R. White and David A. Huse, Phys. Rev. B **48**, 3844 (1993); Tai-Kai Ng, Phys. Rev. B **50**, 555(1994).

¹³ P. Lecheminant and E. Orignac, Phys. Rev. B **65**, 174406 (2002).

¹⁴ Xie Chen, Zheng-Cheng Gu, Xiao-Gang Wen, Phys. Rev. B **83**, 035107 (2011); arXiv:1103.3323.

¹⁵ Xie Chen, Zheng-Cheng Gu, Zheng-Xin Liu, Xiao-Gang Wen, arXiv:1106.4772.

¹⁶ A. P. Schnyder, S. Ryu, A. Furusaki, and A. W. W. Ludwig, Phys. Rev. B **78**, 195125 (2008); A. Kitaev, AIP Conf. Proc. **1134**, **22** (2008); X. G. Wen, Phys. Rev. B **85**, 085103 (2012).

¹⁷ Lukasz Fidkowski, Alexei Kitaev, Phys. Rev. B **81**, 134509 (2010); Phys. Rev. B **83**, 075103 (2011).

¹⁸ E. Tang, X.-G. Wen, Phys. Rev. Lett. **109**, 096403 (2012).

- ¹⁹ X. L. Qi, (2012), arXiv:1202.3983; S. Ryu and S.-C. Zhang, Phys. Rev. B **85**, 245132 (2012); H. Yao and S. Ryu, (2012), arXiv:1202.5805.
- ²⁰ Zheng-Cheng Gu, Xiao-Gang Wen, arXiv:1201.2648.
- ²¹ Z.-X. Liu, M. Liu, and X.-G. Wen, Phys. Rev. B **84**, 075135 (2011); Z.-X. Liu, X. Chen, and X.-G. Wen, Phys. Rev. B **84**, 195145 (2011).
- ²² The anisotropic Heisenberg exchange interactions $J_x S_i^x S_j^x + J_y S_i^y S_j^y + J_z S_i^z S_j^z$ considered in this paper actually have a larger symmetry group, $D_2 \times \sigma \times T$. The full symmetry group $D_2 \times \sigma \times T$ has 128 different projective representations that correspond to one trivial phase and 127 non-trivial SPT phases. All of these phases can be realized in spin ladders, but only part of them can be realized in two-legged ladders. The t_0, t_x, t_y, t_z phases discussed in this paper belong to the 127 non-trivial phases.
- ²³ The three phases t_x, t_y, t_z have similar properties with the T_x, T_y, T_z phases, respectively, discussed in Ref. [21](#) for spin-1 chain models.
- ²⁴ G. Vidal, Phys. Rev. Lett. **91**, 147902 (2003); Phys. Rev. Lett. **93**, 040502 (2004); Phys. Rev. Lett. **98**, 070201 (2007).
- ²⁵ For instance, see M. den Nijs and K. Rommelse, Phys. Rev. B **40**, 4709 (1989); W. Chen, K. Hida and B. C. Sanctuary, Phys. Rev. B **67**, 104401 (2003).
- ²⁶ H. Nonne, E. Boulat, S. Capponi and P. Lecheminant, Phys. Rev. B **82**, 155134 (2010).
- ²⁷ E. Čížmár, *et.al*, arXiv:1005.1474; B. Bleaney and D.K. Bowers, Proc. Roy. Soc (London) **A214**, 451 (1952).
- ²⁸ Michael J. Hartmann, Fernando G. S. L. Brandão, and Martin B. Plenio, Laser & Photon. Rev. **2**, 527 (2008); J. Cho, D. G. Angelakis, and S. Bose, Phys. Rev. A **78**, 062338 (2008).
- ²⁹ S. B. Zheng, and G. C. Guo, Phys. Rev. Lett **85**, 2392 (2000); S. Osnaghi, P. Bertet, A. Auffeves, P. Maioli, M. Brune, J. M. Raimond, and S. Haroche, *ibid* **87**, 037902 (2001).
- ³⁰ A. D. Boozer, A. Boca, R. Miller, T. E. Northup, and H. J. Kimble, Phys. Rev. Lett **97**, 083602 (2006); A. D. Boozer, A. Boca, R. Miller, T. E. Northup, and H. J. Kimble, *ibid* **98**, 193601 (2007).
- ³¹ J. Bochmann, M. Mücke, C. Guhl, S. Ritter, G. Rempe, and D. L. Moehring, Phys. Rev. Lett **104**, 203601 (2010); R. Gehr, J. Volz, G. Dubois, T. Steinmetz, Y. Colombe, B. L. Lev, R. Long, J. Estève, and J. Reichel, *ibid* **104**, 203602 (2010).
- ³² J. Cho, Dimitris G. Angelakis, and S. Bose, Phys. Rev. A **78**, 062338 (2008).